Environmental and genetic factors support the dissociation between α-synuclein aggregation and toxicity

Anna Villar-Piqué[a,1], Tomás Lopes da Fonseca[a,1], Ricardo Sant'Anna[b,c,d], Éva Mónika Szegö[a], Luis Fonseca-Ornelas[e], Raquel Pinho[a], Anita Carija[c], Ellen Gerhardt[a], Caterina Masaracchia[a], Enrique Abad Gonzalez[f,g], Giulia Rossetti[f,h], Paolo Carloni[f], Claudio O. Fernández[i,j], Debora Foguel[b], Ira Milosevic[k], Markus Zweckstetter[e,l,m,n], Salvador Ventura[c,d], and Tiago Fleming Outeiro[a,o,2]

[a]Department of Neurodegeneration and Restorative Research, University Medical Centre Göttingen, 37073 Goettingen, Germany; [b]Instituto de Bioquímica Médica Leopoldo de Meis, Universidade Federal do Rio de Janeiro, 21941-901 Rio de Janeiro, Brazil; [c]Institut de Biotecnologia i de Biomedicina, Universitat Autònoma de Barcelona, 08193 Bellaterra, Barcelona, Spain; [d]Departament de Bioquímica i Biologia Molecular, Facultat de Biociències, Universitat Autònoma de Barcelona, 08193 Bellaterra, Barcelona, Spain; [e]Max-Planck-Institut für Biophysikalische Chemie, 37077 Goettingen, Germany; [f]Computational Biomedicine, Institute for Advanced Simulation IAS-5 and Institute of Neuroscience and Medicine INM-9, Forschungszentrum Jülich, 52425 Jülich, Germany; [g]German Research School for Simulation Sciences, Forschungszentrum Jülich, 52425 Jülich, Germany; [h]Department of Oncology, Hematology, and Stem Cell Transplantation, Medical School, Rheinisch-Westfälische Technische Hochschule Aachen University, 52074 Aachen, Germany; [i]Max Planck Laboratory for Structural Biology, Chemistry, and Molecular Biophysics of Rosario, Universidad Nacional de Rosario, Ocampo y Esmeralda, S2002LRK Rosario, Argentina; [j]Instituto de Investigaciones para el Descubrimiento de Fármacos de Rosario UNR-Consejo Nacional de Investigaciones Científicas y Técnicas de Argentina, Universidad Nacional de Rosario, Ocampo y Esmeralda, S2002LRK Rosario, Argentina; [k]European Neuroscience Institute, 37077 Goettingen, Germany; [l]Deutsches Zentrum für Neurodegenerative Erkrankungen, 37075 Goettingen, Germany; [m]Department of Neurology, University Medicine Göttingen, 37073 Goettingen, Germany; [n]Center for Nanoscale Microscopy and Molecular Physiology of the Brain, University Medicine Göttingen, 37075 Goettingen, Germany; and [o]Max Planck Institute for Experimental Medicine, Goettingen, Germany

Edited by Gregory A. Petsko, Weill Cornell Medical College, New York, NY, and approved September 2, 2016 (received for review April 28, 2016)

Synucleinopathies are a group of progressive disorders characterized by the abnormal aggregation and accumulation of α-synuclein (aSyn), an abundant neuronal protein that can adopt different conformations and biological properties. Recently, aSyn pathology was shown to spread between neurons in a prion-like manner. Proteins like aSyn that exhibit self-propagating capacity appear to be able to adopt different stable conformational states, known as protein strains, which can be modulated both by environmental and by protein-intrinsic factors. Here, we analyzed these factors and found that the unique combination of the neurodegeneration-related metal copper and the pathological H50Q aSyn mutation induces a significant alteration in the aggregation properties of aSyn. We compared the aggregation of WT and H50Q aSyn with and without copper, and assessed the effects of the resultant protein species when applied to primary neuronal cultures. The presence of copper induces the formation of structurally different and less-damaging aSyn aggregates. Interestingly, these aggregates exhibit a stronger capacity to induce aSyn inclusion formation in recipient cells, which demonstrates that the structural features of aSyn species determine their effect in neuronal cells and supports a lack of correlation between toxicity and inclusion formation. In total, our study provides strong support in favor of the hypothesis that protein aggregation is not a primary cause of cytotoxicity.

α-synuclein | copper | H50Q mutation | inclusions | protein aggregation

Synucleinopathies are a group of neurodegenerative disorders that include Parkinson's disease (PD), dementia with Lewy bodies, and multiple system atrophy. Although the clinical manifestations in these disorders are heterogeneous, ranging from movement impairment to dementia, they all share the abnormal accumulation of α-synuclein (aSyn) in proteinaceous inclusions (1). The vast majority of synucleinopathy cases are sporadic. Nevertheless, mutations in the gene encoding for human aSyn have been reported in both familial and sporadic forms of synucleinopathies. In addition to gene multiplications, six point-mutations have been described to cause familial forms of PD: A30P, E46K, H50Q, G51D, A53T, and A53E (2, 3).

aSyn is a soluble 140-residue intrinsically disordered protein that is abundant in neuronal cells, in particular in presynaptic terminals (4). The primary sequence of aSyn can be divided into three regions: (*i*) the N-terminal domain, with strong propensity to adopt α-helical structure, responsible for membrane binding; (*ii*) the central region, known as nonamyloid component, displays high aggregation propensity and is crucial for the amyloidogenicity of the entire protein; and (*iii*) the C-terminal region, highly acidic and disordered, described as a chaperone-like domain (5). Although the biological function of aSyn is still not well understood, increasing evidence suggests it plays a major role in the synapse, where it regulates synaptic vesicle release upon functional multimerization (6). Remarkably, all pathological point-mutations are located in the N-terminal region, required for membrane interactions (3).

Misfolding and aggregation of aSyn is a central event in synucleinopathies. In the case of PD and dementia with Lewy bodies,

Significance

Many neurodegenerative diseases are characterized by the abnormal accumulation of aggregated proteins in the brain. In Parkinson's disease and related disorders, this process involves the accumulation of α-synuclein (aSyn). Thus, understanding the relationship between aSyn aggregation and pathological conditions is essential for the development of novel and efficient therapies against these disorders. Here, we studied the effects that different aSyn species have on neurons using a combination of neurodegeneration-associated factors: the H50Q aSyn mutant and the presence of copper. Importantly, we demonstrate that exogenous aSyn promotes toxicity and inclusion formation, and that these effects are inversely correlated. Our data shed light onto the pathological mechanisms associated with aSyn aggregation, forming the foundation for future therapeutic strategies.

Author contributions: A.V.-P., T.L.d.F., S.V., and T.F.O. designed research; A.V.-P., T.L.d.F., R.S., É.M.S., L.F.-O., R.P., A.C., E.G., E.A.G., G.R., and I.M. performed research; C.M., P.C., C.O.F., D.F., I.M., M.Z., S.V., and T.F.O. contributed new reagents/analytic tools; A.V.-P., T.L.d.F., R.S., É.M.S., L.F.-O., G.R., P.C., C.O.F., D.F., I.M., M.Z., S.V., and T.F.O. analyzed data; and A.V.-P., S.V., and T.F.O. wrote the paper.

The authors declare no conflict of interest.

This article is a PNAS Direct Submission.

[1]A.V.-P. and T.L.d.F. contributed equally to this work.

[2]To whom correspondence should be addressed. Email: touteir@gwdg.de.

This article contains supporting information online at www.pnas.org/lookup/suppl/doi:10.1073/pnas.1606791113/-/DCSupplemental.

aSyn accumulates mainly in intraneuronal inclusions called Lewy bodies (LBs) and Lewy neurites (LNs) (7). The major component of these inclusions is aggregated and phosphorylated aSyn on serine 129 (S129) (8), which adopts fibrillar morphology compatible with that of amyloids (7). LBs and LNs are abundant in various regions of diseased brains, such as the midbrain, hippocampus, and cortex, which exhibit neuronal cell loss and degeneration (9, 10). The mechanisms triggering aSyn aggregation are not clear, nor is the relationship of aSyn aggregation with pathology. Several theories attempt to explain the toxicity of misfolded/aggregated aSyn, including the impairment in the endoplasmic reticulum trafficking pathway, dysfunction of mitochondria, blocking of protein clearance mechanisms, alteration of axonal transport, and disruption of the plasma membrane (11–13). The precise nature of the toxic aSyn species is still unclear, although it is believed that specific oligomeric species might be cytotoxic, rather than the mature aggregates (14, 15).

Based on the Braak staging hypothesis (16) and on the observation of LB pathology in young dopaminergic neurons grafted into the brains of PD patients (17), it was proposed that aSyn pathology might spread in a prion-like manner. Subsequently, in vitro and in vivo studies confirmed the ability of aSyn to be released/secreted and taken up by neighboring cells (18–20), further supporting the prion-like spreading of aSyn.

Environmental factors, such as exposure to pesticides or metals, are thought to increase the risk for PD and, possibly, other synucleinopathies (21, 22). Indeed, deregulation of metal homeostasis, including copper, manganese, zinc, iron, and lead, is characteristic of these disorders (23, 24). However, there is still no unequivocal evidence for a causative role of metals in synucleinopathies. In particular, the precise relationship between those metals and aSyn in the brain is not clear, although they bind to and promote the aggregation of the protein in vitro (25, 26).

In the present study, we systematically screened for the effect of transition metals on the intracellular aggregation of disease-associated aSyn mutants and found a significant effect of copper(II) ions (Cu^{2+}) on the H50Q mutant. We produced recombinant aggregates from WT and H50Q aSyn variants in the presence and absence of Cu^{2+}, performed detailed biophysical and structural analyses, and assessed their impact on neuronal cells. Importantly, our studies of the interplay between environmental and genetic factors affecting aSyn aggregation support dissociation between cytotoxicity and intracellular aggregation, forming the basis for future studies aimed at targeting specific species of aSyn as therapeutic strategies.

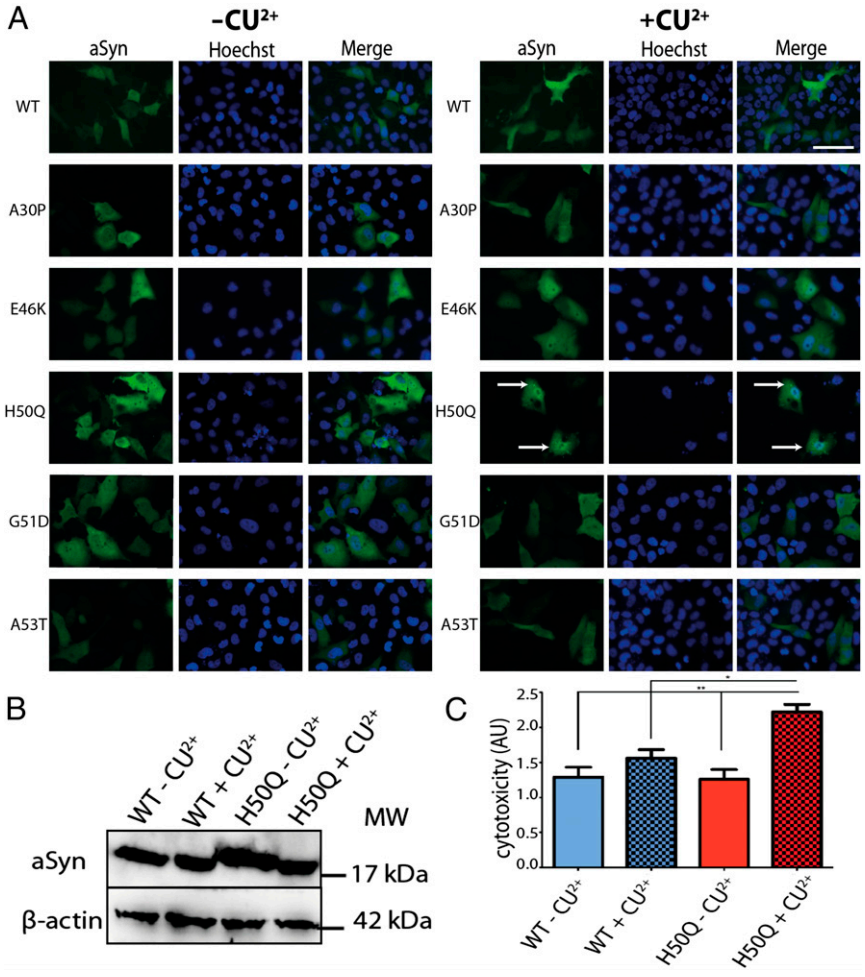

Fig. 1. Copper ions promote the intracellular accumulation of H50Q aSyn inclusions. (*A*) The addition of Cu^{2+} to the medium of cells transfected with different aSyn mutations revealed the formation of intracellular inclusions only in the presence of the H50Q aSyn mutant (white arrows). (Scale bar, 5 μm.) (*B*) The effect observed was not associated with an increase in intracellular levels of expression of the H50Q mutant, as determined by immunoblot analysis. (*C*) The interaction between Cu^{2+} and H50Q promotes an increase in cytotoxicity compared with WT $-Cu^{2+}$, WT $+Cu^{2+}$, and H50Q $-Cu^{2+}$. MW, molecular weight/molecular mass. $^{*}P < 0.05$; $^{**}P < 0.01$.

Results

Copper(II) Induces H50Q aSyn Aggregation in Human Cells. Transition metals, such as copper, interact with aSyn and modify its aggregation properties (26). To assess the interplay between Cu^{2+} and aSyn mutations, we took advantage of an established cell model of aSyn aggregation in human H4 neuroglioma cells and used it as a system to screen the effect on five disease-associated aSyn mutants. We supplemented the cell culture medium with $CuCl_2$ 24 h after transfection with plasmids encoding for the different aSyn mutants and incubated cells for 24 h. Upon immunohistochemistry and microscopy analysis we observed that Cu^{2+} promoted the formation of intracellular inclusions with the H50Q aSyn (Fig. 1*A*). This effect was not because of a change in the levels of expression of the H50Q mutant, which remained identical to those of WT aSyn (Fig. 1*B*). Interestingly, we observed an increase in cytotoxicity in cells expressing H50Q in the presence of Cu^{2+} (Fig. 1*C*). Importantly, the effect of Cu^{2+} on the H50Q aSyn mutant appears to be specific to this cation, because other relevant transition metals (24) did not induce the formation of aSyn inclusions (*SI Appendix*, Fig. S1). Therefore, we decided to focus our studies on the characterization of the interplay between H50Q aSyn and Cu^{2+}.

The Effect of Cu^{2+} on aSyn Aggregation in Vitro. First, we evaluated the effect of Cu^{2+} on the aggregation of WT and H50Q aSyn (Fig. 2*A*). The kinetics of amyloid fibril formation usually follows a sigmoidal curve that reflects a nucleation-dependent growth mechanism (27). Both in the absence and presence of Cu^{2+}, WT aSyn aggregation followed this kinetics. In the absence of Cu^{2+}, the WT aSyn reaction (WT $-Cu^{2+}$) exhibited a long lag phase of ∼100 h followed by a fast increase in thioflavin-t (Th-T) signal that reached maximum fluorescence intensity after ∼250 h of incubation in the conditions tested. The presence of Cu^{2+} (WT $+Cu^{2+}$) accelerated the aggregation reaction, shortening the lag phase to ∼50 h and, consistently, the equilibrium was reached at ∼200 h. We found a distinct scenario with the H50Q mutant. Although the aggregation of H50Q in the absence of Cu^{2+} (H50Q $-Cu^{2+}$) also followed a typical sigmoidal curve, the lag phase was shorter than for WT aSyn (∼25 h), followed by an exponential phase that plateaued at ∼90 h. In contrast, in the presence of Cu^{2+} (H50Q $+Cu^{2+}$), aggregation was strikingly faster, lacking a detectable lag phase, and Th-T signal remained very weak throughout the reaction, suggesting either the formation of nonfibrillar amyloid species or reduced aggregation. For WT aSyn, the presence of Cu^{2+} led to an increase in Th-T binding at the end of the reaction, whereas for the H50Q mutant it resulted in the opposite effect (Fig. 2*B*). To further confirm that the four samples aggregated and, especially, that the weak Th-T signal in H50Q + Cu^{2+} did not correspond to a marked reduction in the amount of deposited protein, we performed a sedimentation assay, measuring the protein remaining in the supernatant after centrifugation. In this assay, all samples showed similar amounts of insoluble material (Fig. 2*C*), despite the differential binding to Th-T. Finally, we assessed the potential dependence of aSyn aggregation on Cu^{2+} concentration, from sub- to suprastoichiometric concentrations, using the Th-T-binding assay. With both aSyn variants, an increase in Cu^{2+} concentration caused a shortening of the lag phase, although this effect was limited to the equimolar ratio. Exposing aSyn to suprastoichiometric Cu^{2+} concentration did not significantly accelerate the aggregation kinetics of WT or H50Q (*SI Appendix*, Fig. S2) relative to an equimolar ratio. Another neurodegeneration-related metal, iron, was introduced in the aggregation assay, but no effect was observed, indicating that the effect of Cu^{2+} on aSyn aggregation is probably specific for this cation (*SI Appendix*, Fig. S2).

Next, we performed biophysical characterization of the resulting aggregates using circular dichroism (CD), attenuated total reflectance–Fourier transform infrared spectroscopy (ATR–FTIR), 1-anilinonaphthalene-8-sulfonic acid (ANS) binding, and transmission electron microscopy (TEM). We analyzed the secondary structure of the samples by CD before and after aggregation. As expected, freshly prepared aSyn samples, in the presence or absence of Cu^{2+}, exhibited a characteristic negative CD peak at 200 nm, consistent with the lack of significant secondary structure in aSyn, because it is known to be an intrinsically disordered protein (*SI Appendix*, Fig. S3*A*). After aggregation, the CD spectra strongly changed, showing a minimum at around 216 nm, consistent with the presence of β-sheet structure. Deconvolution of the ATR–FTIR raw spectra of aggregated states into the corresponding contributing components ($r^2 < 0.998$ in all cases) indicated that both WT $-Cu^{2+}$ and WT $+Cu^{2+}$ shared similar secondary structure elements (*SI Appendix*, Fig. S3*B*). The peak at 1,623–1,641 cm^{-1}, assignable to intermolecular β-sheet structure, dominated both spectra (Table 1). However, the ratio between the β-sheet and the disordered spectral component was higher in the absence than in the presence of Cu^{2+} (2.0 and 1.3). The intermolecular β-sheet component was also the main contributor to the H50Q $-Cu^{2+}$ spectra with a ratio between this signal and that of the disordered state similar to that observed with WT $-Cu^{2+}$ (1.9). In contrast, in the case of H50Q $+Cu^{2+}$, the intermolecular β-sheet signal did not dominate the spectra but contributed the same amount as the disordered regions (ratio of 1.0) with an additional increase in β-turn content by 27%. Thus, the presence of Cu^{2+} resulted in fewer ordered aggregates for both the WT and the H50Q mutant, but the decrease in β-structure was more pronounced for H50Q aSyn. Structural differences of the

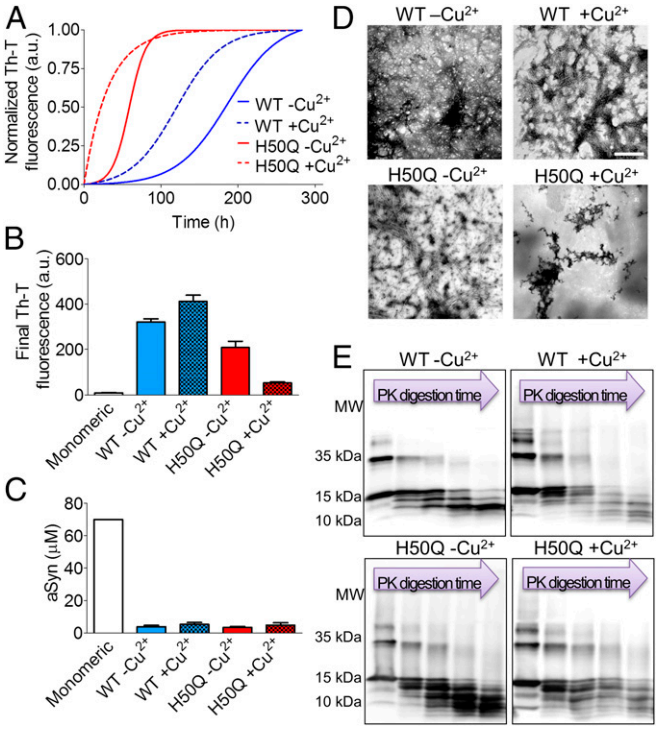

Fig. 2. Biophysical characterization of the effect of copper ions on the aggregation of WT and H50Q aSyn. (*A*) Aggregation kinetics of WT and H50Q aSyn with and without Cu^{2+} evaluated by normalized Th-T binding at the indicated time points. Fluorescence intensity peak at 482 nm was used to probe for amyloid formation. (*B*) Fluorescence intensity at the end-time point of the Th-T binding assay. (*C*) Remaining amount of soluble aSyn determined by sedimentation assay at the end time point of aggregation. (*D*) TEM images of the resulting aggregates stained with uranium acetate. (Scale bar, 500 nm.) (*E*) Partial PK digestion of the aggregates visualized by Coomasie staining of SDS/PAGE gels. Each lane represents different digestion times: 0, 1, 2.5, 5, and 10 min.

Table 1. Secondary structure composition of the fibrils formed by WT $-Cu^{2+}$, WT $+Cu^{2+}$, H50Q $-Cu^{2+}$ and H50Q $+Cu^{2+}$

Sample	β-Sheet intermolecular	Disordered	Turns
WT $-Cu^{2+}$	56.73	27.63	15.63
WT $+Cu^{2+}$	46.10	36.33	17.56
H50Q $-Cu^{2+}$	54.61	29.06	16.32
H50Q $+Cu^{2+}$	38.97	39.17	21.84

The assignments are represented in percentage and were attributed to each peak observed according to Susi and Byler (75).

aggregates were also determined using the ANS binding assay (*SI Appendix*, Fig. S3*C*). With both aSyn variants, the presence of Cu^{2+} increased the ANS fluorescence of the aggregates (more than 1.5-fold and 3-fold increase in WT and H50Q, respectively), suggesting that Cu^{2+} increased the exposure of hydrophobic surfaces in the resulting aggregates. The initial soluble species did not show differences in ANS binding among them, suggesting that the impact of Cu^{2+} on the exposure of hydrophobic clusters in aSyn assemblies occurs during the aggregation process. The morphology of the aggregated samples was further investigated by TEM (Fig. 2*D*). Both WT $-Cu^{2+}$ and WT $+Cu^{2+}$ formed well-defined and classic amyloid filaments. This scenario was different for the H50Q mutant, where the presence of Cu^{2+} induced the formation of nonfibrillar amorphous aggregates. Overall, the secondary structure found in the aggregates and their morphology correlated well with their relative ability to bind Th-T and is indicative of a different conformational effect of Cu^{2+} in WT and in H50Q aSyn. In addition, we examined the resistance of each aSyn aggregate to proteolysis by performing a time-dependent partial proteinase K (PK) digestion. We found that the species assembled in presence of Cu^{2+} displayed decreased resistance to proteolysis, whereas those formed without Cu^{2+} exhibited a strongly resistant core (Fig. 2*E*). Notably, in all cases the most susceptible region was the C terminus, as evidenced by the use of an antibody recognizing this region of the protein (*SI Appendix*, Fig. S4).

Because spreading of disease pathology might depend on the ability of the transmitted protein to seed aggregation in the recipient cell, we investigated the capacity of the aggregates of WT and H50Q aSyn, formed in the absence and presence of Cu^{2+}, to influence the aggregation of monomeric aSyn. To this end, the time-dependent decrease in the concentration of monomeric aSyn was monitored using NMR spectroscopy, which allows the highly sensitive detection of the initial steps of aggregation. Species formed without Cu^{2+} displayed a strong seeding activity, rapidly decreasing the amount of free monomers in solution. However, this activity was reduced when the aggregates formed in the presence of Cu^{2+} were used as seeds. Indeed, H50Q $+Cu^{2+}$ did not induce significant monomer consumption, indicating the absence of seeding activity at the time points analyzed (Fig. 3).

aSyn–Cu^{2+} Complexes at the Histidine 50 Site. Because the histidine 50 (H50) residue is key for anchoring Cu^{2+} binding to aSyn, the results suggested that the critical step for the effects observed in Cu^{2+}-mediated aSyn aggregation might be the formation aSyn–Cu^{2+} complexes at this site. In vitro NMR (28) and electron paramagnetic resonance (26, 29) experiments have suggested that the ion binds in a square planar or tetrahedral distorted geometry, involving 2 or 3 N ligands and 2 or 1 O ligands, respectively (29–31). Models A and B (*SI Appendix*, *SI Molecular Simulations*) have been proposed in the literature (28, 29, 32). The Cu^{2+} ion binds to the H50 side chain in both of them. The three additional ligands are the H50 amide group, a water molecule, and either V48 carbonyl O (model A) or V49 deprotonated amide (model B). Quantum mechanics/molecular mechanics simulations were carried out to test their structural stability (*SI Appendix*, *SI Molecular Simulations*). All of the coordination bonds exhibited relatively small fluctuations around their average values, except for the Cu^{2+}–V48 carbonyl and Cu^{2+}–V49 amide. This finding suggests an interconversion between the two forms. Added to the models in which H50 participation in binding to aSyn would involve the formation of an intramolecular macrochelate or would lead to intermolecular metal-bridged protein molecules (33), our calculations suggested that: (*i*) both models could be significantly populated binding modes; (*ii*) aSyn conformation is preorganized to accommodate the square planar conformation of Cu^{2+}, suggesting the latter may bind using a conformational selection mechanism (34); and (*iii*) Cu^{2+} is able to bind independently to the imidazole nitrogen of H50 in a N2O2 (A) or N3O1 (B) interconverting ligand donor sets, with the additional ligands mentioned above. In contrast, the H50Q variant lacks all these modes of Cu^{2+} binding, indicating differences with the WT protein, possibly underlying different conformations. Other models, initially considered, were discarded (*SI Appendix*, *SI Molecular Simulations*).

aSyn Aggregates Are Cytotoxic When Applied to Primary Neuronal Cultures. The aSyn aggregates we generated in the various conditions had distinct conformational and seeding properties. Thus, we next asked whether they might have differential effects when applied to cultured cells. We exposed rat primary cortical cultures for 13 d to the species resulting from aSyn aggregation. We found that all aSyn species were toxic on neuronal cultures as assessed by the release of adenylate kinase to the medium because of cell damage (Fig. 4*A*). Quantification of the remaining cells and of the percentage of condensed nuclei also revealed cell loss after treatment with aSyn aggregates (Fig. 4 *B* and *C*). Immunostaining against microtubule-associated protein 2 (MAP2) confirmed that the reduced number of cells was a result of neuronal loss. We also found a reduction in the average neurite length, particularly pronounced in the cultures treated with WT $-Cu^{2+}$ and H50Q $-Cu^{2+}$ (Fig. 4*D*). Consistently, these cultures displayed reduced levels of MAP2, as determined by immunoblot analysis (Fig. 4*E*). Because MAP2 is specifically present in dendrites, we also used Tau as an axonal marker of mature neurons (35) to assess whether these projections could also be affected, but found no significant differences (Fig. 4*E*). To measure possible synaptic damage induced by the aSyn aggregates, we quantified the levels of presynaptic (synapsin and synaptophysin) and postsynaptic (postsynaptic density protein 95) markers (*SI Appendix*, Fig. S5). We observed a significant reduction of these markers in cells that were treated with WT $-Cu^{2+}$ and H50Q $-Cu^{2+}$. Because the application of

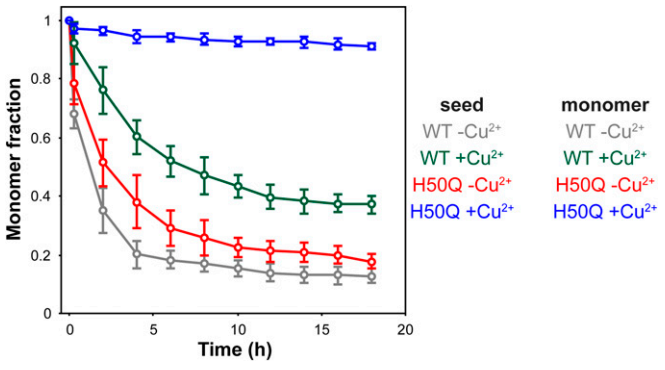

Fig. 3. Copper ions reduce the seeding capacity of aSyn aggregates. Time-dependence of 1H NMR spectra of monomeric aSyn upon addition of aggregation seeds [4% (vol/vol)]. The integrated intensity of ^{1}H signals in two regions (0.50–1.05 ppm, 6.50–8.00 ppm) was calculated and plotted as a function of time. The solution with 70-μM monomeric protein (WT or H50Q) contained either no Cu^{2+} or an equimolar concentration of Cu^{2+}, as indicated.

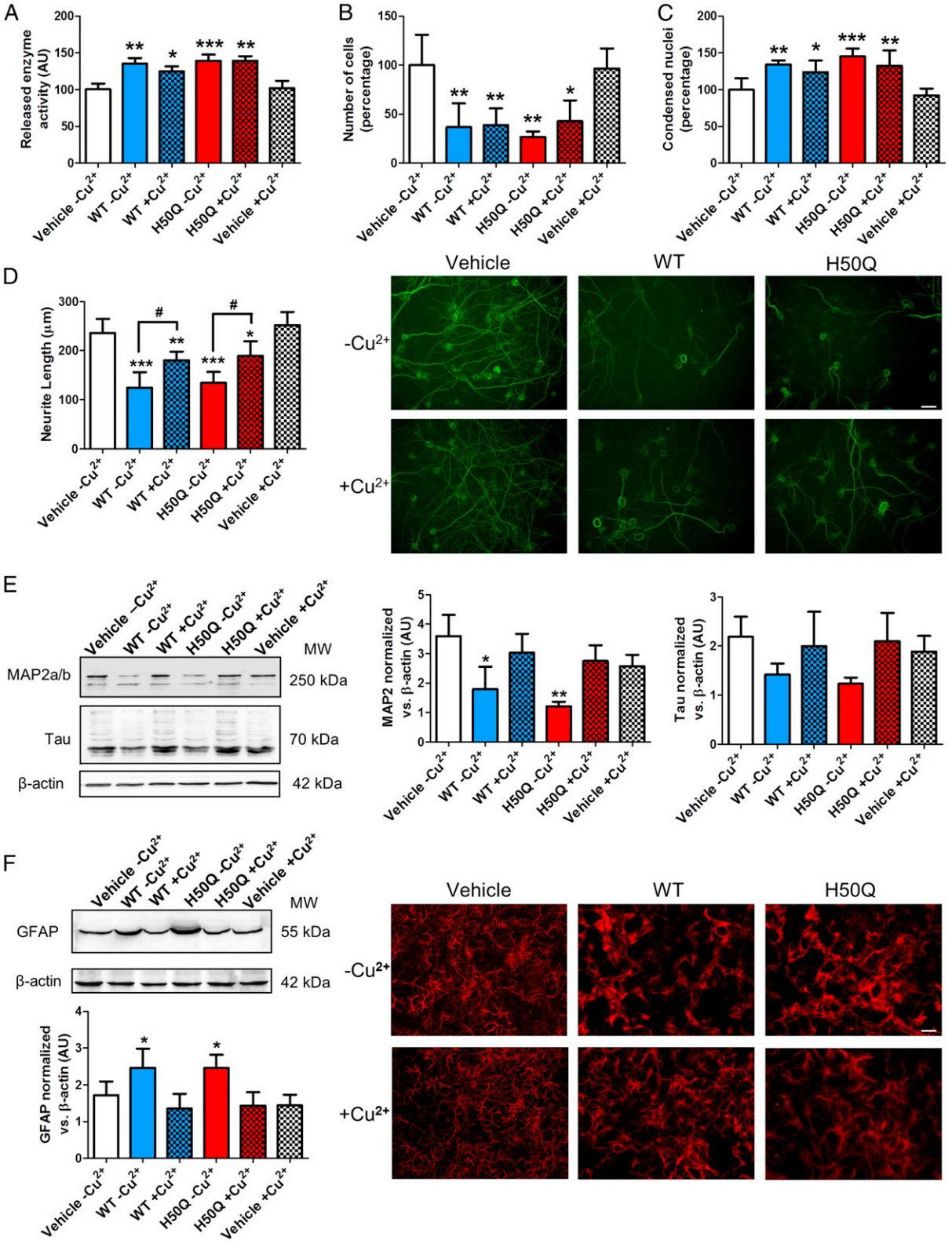

Fig. 4. Cellular effects as a result of the exogenous application of aSyn aggregates. (*A*) Cytotoxicity quantification in cultures exposed to aggregates compared with the vehicle control, measured as the presence of adenylate kinase in the medium. (*B*) Cell death quantification, measured as the reduction in the number of cells. (*C*) Increase in the percentage of condensed nuclei in the same experiment represented in *B*. (*D*) Quantification of neurite length of cells exposed to aggregates compared with the vehicle control (*Left*) and representative images of MAP2 stained cultures, used to obtain the former parameter (*Right*). (Scale bars, 20 μm.) (*E*) Quantification of MAP2 and Tau levels by Western blot. (*F*) Astrogliosis caused by the application of aSyn aggregates, measured by Western blot quantification of GFAP (*Left*), and representative images evidencing the presence of reactive astrocytes (*Right*). (Scale bars, 20 μm.) $^{*}P < 0.05$; $^{**}P < 0.01$; $^{***}P < 0.001$ for comparison between samples and their appropriate vehicle control. $^{\#}P < 0.05$; $^{\#}P < 0.01$ for comparison between different samples.

pathological aSyn species has been reported to induce a glial response in vivo (20, 36), we investigated the state of the astrocytes by probing for glial fibrillary acidic protein (GFAP). An increase in GFAP levels could only be detected in cells exposed to WT $-Cu^{2+}$ and H50Q $-Cu^{2+}$, likely because of the development of reactive astrocytes, as GFAP staining revealed a phenotype compatible with reactive astrocytes (37) (Fig. 4*F*).

Overall, we demonstrated that aggregated recombinant aSyn species promoted neuronal death and damage. Importantly, the effects observed depended on the type of aggregate that was used, being more acute in the case of aggregates formed without Cu^{2+}.

aSyn Aggregates Induce the Formation of Phosphorylated aSyn Inclusions. Next, we analyzed the capacity of the different aggregated species of aSyn to induce the conversion of endogenous aSyn into misfolded/aggregated forms in cultured cells. The experimental set-up was the same as described above. We performed immunostaining with an antibody against phosphorylated aSyn (p-aSyn) on S129, because aggregated aSyn is commonly phosphorylated in this residue, as in LBs (8). This approach also enabled us to specifically detect intracellular aSyn, and not external protein, as this was not phosphorylated and, therefore, could not react with the antibody against p-aSyn (38). Although we observed a wide distribution of p-aSyn in the cell body of vehicle-treated cells (Fig. 5*A*), those exposed to aSyn aggregates displayed more intense and concentrated signal, corresponding to inclusions positive for p-aSyn (Fig. 5*A*). Cells treated with H50Q $-Cu^{2+}$, and particularly with WT $-Cu^{2+}$ species, contained fewer inclusions. In contrast, those treated with WT $+Cu^{2+}$ and H50Q $+Cu^{2+}$ presented several p-aSyn^{+} inclusions, which we classified as neuritic, perykarial, and nuclear (Fig. 5*B*). Because of technical limitations in the quantification of inclusions in neurites, we performed a semiquantitative assessment of the frequency of all types of inclusions in Table 2. We also performed quantification of total p-aSyn on S129 by immunoblot (Fig. 5*C*). Strikingly, the occurrence of intracellular inclusions was highly specific to the type of aggregates applied to the cells. We observed neuritic inclusions in all treatments, although very few were observed in cells treated with WT $-Cu^{2+}$ and H50Q $-Cu^{2+}$. With the latter treatment (H50Q $-Cu^{2+}$), we also observed dispersed perykarial inclusions. Cultures treated with aggregates formed in the presence of Cu^{2+} presented more inclusions in neurites and perykaria. Specifically, cells treated with H50Q $+Cu^{2+}$ displayed the largest number of all types of inclusions (Table 2). To rule out issues of unspecificity of the p-aSyn antibody (39), we validated the observed staining with an antibody against total aSyn (*SI Appendix*, Fig. S6). The insoluble nature of the induced p-aSyn inclusions was confirmed using an established fixation protocol during the immunostaining that included the presence of Triton X-100 to remove soluble proteins and structures (38). Furthermore, detection of cellular aSyn in the insoluble fraction in the cultures displaying more inclusions (those treated with WT $+Cu^{2+}$ and H50Q $+Cu^{2+}$) corroborated the presence of aggregated aSyn (Fig. 5*D*).

We next aimed at determining which particular aSyn protein composed the inclusions observed. The use of an antibody specific for rat aSyn revealed that part of the inclusions present in neurites and perykaria are mainly formed by human recombinant protein that was internalized, whereas all nuclear inclusions were made up of endogenous aSyn (Fig. 6*A*). To further investigate the presence of exogenous aSyn in the nuclear inclusions, we labeled the aggregates formed by H50Q $+Cu^{2+}$ in vitro, as those were the most active in promoting these types of inclusions, and applied them to the cells using the same procedure as above. Immunostaining against p-aSyn confirmed the absence of exogenous aSyn in the nuclear inclusions (Fig. 6*B*). To unequivocally validate this finding, labeled aSyn species were applied to neurons expressing GFP and live cell imaging was performed. Recombinant material was internalized into the cells, but was unable to cross the

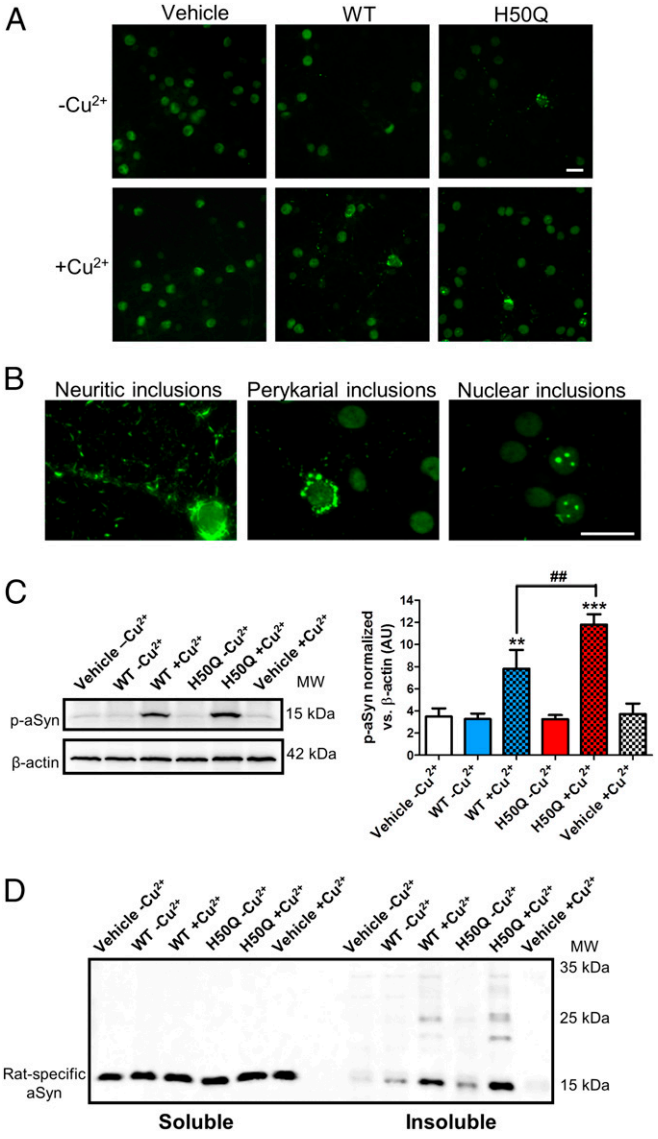

Fig. 5. Formation of S129 p-aSyn^{+} inclusions upon exposure to aSyn aggregates. (*A*) Representative images of each culture showing the presence of p-aSyn (S129) inclusions in cells treated with exogenous aggregates. (Scale bars, 20 μm.) (*B*) Distinct types of p-aSyn inclusions classified as neuritic, perykarial and nuclear. (Scale bars, 20 μm.) (*C*) Western blot measurements of p-aSyn (S129) in cell lysates. (*D*) Soluble/insoluble distribution of the cellular aSyn detected with a rat-specific aSyn antibody. $^{**}P < 0.01$; $^{***}P < 0.001$ for comparison between samples and their appropriate vehicle control. $^{\#\#}P < 0.01$ for comparison between different samples.

nuclear membrane (Fig. 6*C*). Therefore, we confirmed that nuclear p-aSyn inclusions were exclusively formed by endogenous aSyn.

We performed further characterization of the p-aSyn^{+} inclusions. On the one hand, inclusions present in neurites were visible in Tau^{+} projections, confirming their axonal localization. They appeared as puncta or short filaments and, part of them, showed a discontinuous linearity that could be followed up to the neuronal cell body (Fig. 5*B* and *SI Appendix*, Fig. S7*A*). On the other hand, perykarial inclusions were examined by costaining with Lamin B1, which stains the nuclear envelope. We confirmed their presence in the cell body and around the cell nucleus (*SI Appendix*, Fig. S7*B*). Both neuritic and perykarial inclusions appeared positive for heat-shock protein 90 (Hsp90), a molecular chaperone commonly present in LBs and other protein

Table 2. Table presenting semiquantification of the frequency of p-aSyn (S129) inclusions in each culture measured from immunostaining pictures

aSyn species	Neuritic	Perykarial	Nuclear
WT $-Cu^{2+}$	+	—	—
WT $+Cu^{2+}$	++	+++	+
H50Q $-Cu^{2+}$	+	+	—
H50Q $+Cu^{2+}$	+++	++	+++

aggregates (40) (*SI Appendix*, Fig. S7 *A* and *B*). Finally, the localization of nuclear inclusions was confirmed by costaining with Hoechst, a widely used nuclear stain. On average, one to six p-aSyn^{+} round structures appeared in the nuclei of cells containing inclusions. These were usually present in areas that were Hoechst^{-}. The lack of costaining with nucleolar markers (nucleolin and fibrillarin) ruled out their presence in the nucleoli (*SI Appendix*, Fig. S7*C*). However, we could detect costaining with ubiquitin, one of the main hallmarks of disease-associated protein deposits (41). Despite the presence of p-aSyn inclusions, we did not detect significant alteration in markers of the heat shock response or of the endoplasmic reticulum stress in our experimental conditions (*SI Appendix*, Fig. S8).

Discussion

PD is characterized by the accumulation of aSyn^{+} fibrillar inclusions, and is associated with an imbalance in metal ion homeostasis (e.g., Cu, Zn, and Fe) (24). In the present study we first screened the effect of Cu^{2+} over different disease-associated aSyn mutants. After the exogenous addition of this cation, H50Q aSyn was the only mutant exhibiting intracellular accumulation. The interplay between this variant and Cu^{2+} was highly specific, because upon testing other relevant metals (24), no H50Q aSyn inclusions were observed. This unique synergy is not surprising, considering that the N-terminal region of aSyn in which H50 acts as a key metal anchoring residue constitutes the preferential binding interface for Cu^{2+} (28, 26, 33, 42). Previous studies, using other cell models, revealed that exposure to Cu^{2+} promotes inclusion formation and toxicity in aSyn-expressing cells (43) and that the H50Q aSyn mutant exhibits a higher aggregation propensity when expressed intracellularly (44). Consistently, in our screen we detected a specific increase in aSyn aggregation only with the combination of H50Q aSyn and Cu^{2+}, an effect that exacerbates cytotoxicity.

In cell-free conditions and in agreement with previous evidence (26), we show here that Cu^{2+} specifically increases the aggregation propensity of WT aSyn, reducing the lag phase and accelerating self-assembly. However, the effect of Cu^{2+} in the aggregation of H50Q aSyn is clearly different from that in the WT protein, resulting in a very rapid formation of amorphous aggregates that—despite containing intermolecular β-sheet structure—bind to Th-T with low affinity, suggesting major structural differences that include, among other features, a larger increase in the exposure of hydrophobic surfaces as revealed by ANS binding. These differences are probably because of the substitution of a key metal binding site (H50) in the H50Q mutant, which mainly coordinates Cu^{2+}, in comparison with other metal cations that may have higher affinities for other residues in the aSyn sequence (45). Despite the reported variability, all aSyn species share a common aggregation core with a less-compacted region mainly composed by the C terminus of the polypeptide. This finding is in agreement with previous data reporting the poor participation of the C-terminal domain in fibril formation, which indeed remains mainly disordered instead of acquiring the typical β-sheet structure (46). The definition of aSyn as a prion-like protein is intimately linked to an intrinsic seeding activity of, at least, some misfolded conformations. We observe that the distinctive structural features introduced by the presence of copper ions are mirrored in differential seeding activities. Among the species tested, the one formed by H50Q $+Cu^{2+}$ is the only one not acting as an efficient seed in our conditions. The aggregates formed by H50Q $+Cu^{2+}$ differ significantly

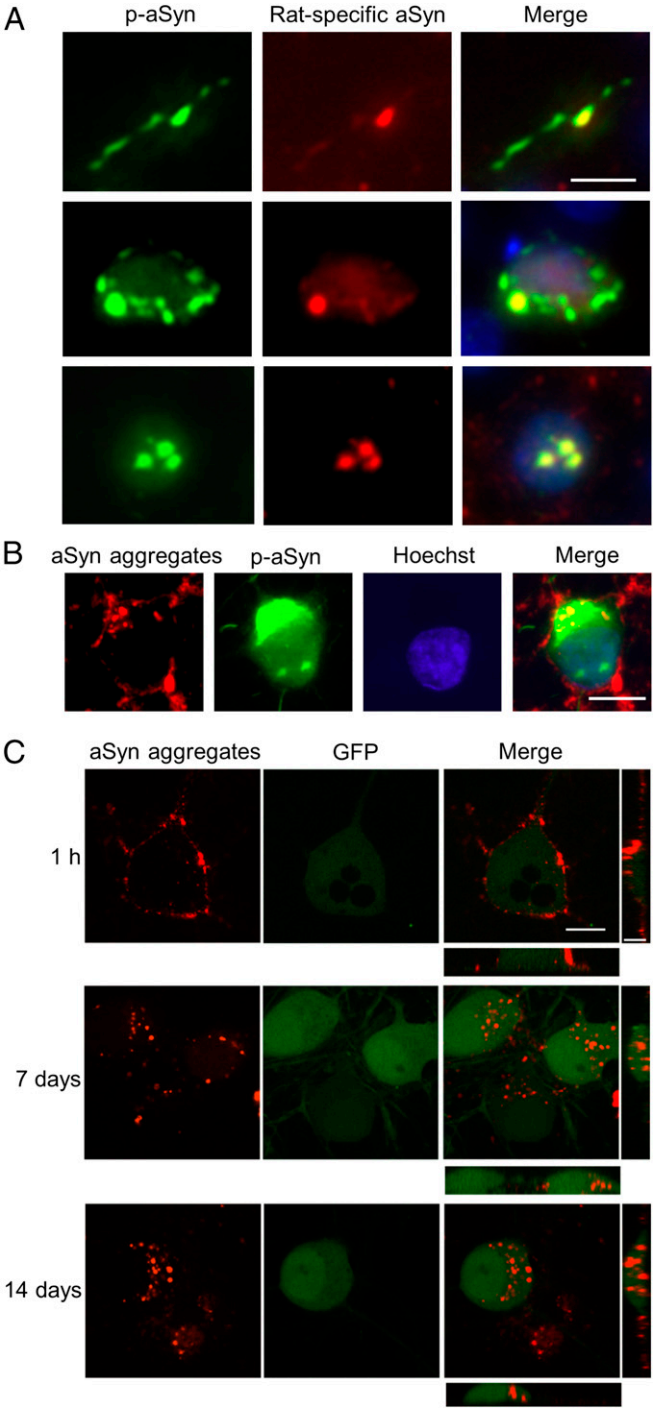

Fig. 6. Distribution of exogenous and endogenous aSyn in the S129 p-aSyn inclusions. (*A*) Neuritic (*Top*), perykarial (*Middle*), and nuclear (*Bottom*) p-aSyn inclusions show partial or total colocalization with rat-specific aSyn. (*B*) Presence and absence of labeled aSyn aggregates in perykarial and nuclear p-aSyn inclusions. (*C*) Confocal live cell imaging of cultures exposed to labeled aSyn aggregates and infected with a GFP-expressing lentivirus demonstrating the cellular distribution of the exogenous species at different time points after exposure. (Scale bars, 10 μm.)

from the other ones, being mainly amorphous, with low Th-T binding and lacking seeding activity. Taken together, these findings show that the combination of the H50Q mutation and Cu^{2+} promotes the formation of atypical aSyn aggregates, probably representing off-pathway species.

As mentioned above, H50 is crucial in the binding of Cu^{2+} to aSyn. Our quantum mechanics/molecular mechanics simulations suggest that the protein backbone and a water molecule complete the coordination of Cu^{2+}. The participation of H50 in metal binding may induce different folding of the protein through the formation of this macrochelate or may act as an intermolecular metal-anchoring point bridging different protein molecules, explaining how H50–Cu^{2+} complexation might impact on aSyn aggregation (33). Added to that, the independent, noninteractive H50–Cu^{2+} binding mode described in our study and those reported for Cu^{+} binding to aSyn (47) indicate that the H50 site constitutes a unique target for in vivo Cu^{2+}/Cu^{+} redox chemistry and oxidative damage, a reaction that might lead to a cascade of structural alterations promoting oligomerization and the subsequent amyloid aggregation of aSyn (33). Thus, H50 might play an important role in the structures adopted by soluble aSyn at the beginning of the aggregation reaction and, likely, of the polymerization rates and the final conformation in the resulting aggregates, which would explain the conformational diversity of WT +Cu^{2+} and H50Q +Cu^{2+} aggregates.

A relevant approach to assess aSyn propagation consists of the induction of aSyn aggregation, upon treatment with preformed fibrils or aggregates, in cultured cells without previous aSyn pathology (48–50). Here we used a similar approach with the objective to further characterize the aSyn species being studied, considering their distinct biophysical features. We used primary neuronal cultures as others have done in the past (51). We found that, although all types of recombinant aSyn aggregates promote cell death, the strongest effect occurs with those assembled in the absence of Cu^{2+}. The specific decrease in neurite length suggests deterioration of neuronal processes precedes cell death. The absence of significant alteration in Tau levels indicates that dendritic arborization is more susceptible to aSyn toxicity than axons. At the end point of our experiments, the axonal network is mature and complex (35), probably exhibiting increased resistance to external insults. The damage induced by aSyn aggregates is also evident in synaptic terminals. However, the toxicity linked to exogenous aSyn is still not fully established, probably because it depends on the cellular type, on the endogenous levels of aSyn, or on the type and properties of the aSyn species used (38, 49, 52–54). In the present study, two of four types of mature aSyn aggregates tested were significantly more toxic, strongly affecting neuronal structures. Interestingly, along with the neuronal damage observed, we also detected reactive astrocytes in our cultures. Our findings are consistent with studies demonstrating that incubation of astrocytic cultures with neuronal-derived aSyn triggered aSyn aggregation in these cells, along with changes in the levels of cytokines and chemokines, a sign of an inflammatory response (55). In our study, the inflammatory response we observe is intimately linked to neuronal damage but independent of inclusion formation.

Furthermore, we investigated the intrinsic capacity of the species tested to induce aSyn aggregation in the recipient cells. The use of an antibody against S129 p-aSyn reveals a basal nuclear aSyn phosphorylation in naïve neurons, compared with a more punctate signal for total aSyn that is mostly present in the neuronal processes. This finding is in agreement with the well-known presynaptic location of aSyn and the enrichment of the phosphorylated form in the nuclear compartment (4, 56). According to previous reports, we found that neurons exposed to aSyn aggregates develop S129 p-aSyn inclusions, displaying increased levels of insoluble aSyn (38, 49). However, in contrast to other studies (39), overexpression of the cellular aSyn or expression of the human form was not required. The inclusions formed could be classified depending on their localization in the cell. Neuritic and perykarial inclusions have also been observed by others (49, 51, 57) and colocalize with Hsp90, resembling pathology-related aggregates (40). These inclusions are formed by both endogenous aSyn and internalized recombinant species. On the other hand, we found nuclear inclusions, which are excluded from the nucleoli. Despite sporadic reports of the occurrence of aSyn aggregates in the nuclei (58, 59), the morphology we observe has not, to the best of our knowledge, been previously described. Nuclear inclusions are ubiquitinated and exclusively formed by endogenous aSyn, as recombinant species were not present in the nuclear compartment. Integrating our findings with data from previous reports (38), aSyn inclusion formation—upon stimulation from the outside—could follow a progression pattern in which exogenous species are internalized, leading to the appearance of inclusions in the projections, and then in the cell body, upon partial sequestration of the endogenous protein. Subsequently, nuclear inclusions appear, likely through a different mechanism because they do not contain detectable amounts of the exogenous protein. Given the apparent lack of seeding capacity of H50Q +Cu^{2+} aggregates in vitro, additional studies will be required to unravel the cellular mechanisms by which endogenous S129 p-aSyn inclusions form in the nucleus, once the cytoplasm has been invaded by exogenous material.

In general, inclusion formation upon aSyn transmission is a phenomenon highly dependent on the type of exogenous species the cell encounters. We found that WT –Cu^{2+} aggregates rarely induce inclusion formation in the cells, in contrast with previous studies (49, 51), possibly because of different experimental approaches. In contrast, cells treated with aggregates formed in the presence of Cu^{2+}, particularly H50Q +Cu^{2+}, promote the formation of the various types of inclusions we identified. However, we cannot explain why previous studies failed to observe nuclear aSyn inclusions. A possible explanation could be the actual nature of the H50Q +Cu^{2+} aggregates, which display different biophysical features. Recent studies suggest that aSyn can adopt various conformations with distinctive characteristics, including distinct propagation capacity (53). These discoveries led to the assumption that aSyn could assemble as different strains in vitro, a hypothesis that has been recently tested in rats (58). In the present study, we demonstrate that structurally different aSyn species exert distinct effects when applied to neuronal cells, and that these effects might be because of the presence of Cu^{2+} during the aggregation process, a situation that may occur in the brain, a result of different environmental stimuli.

A final observation from our experiments is the dissociation between toxicity and inclusion formation, in agreement with other studies (52, 60, 61). WT +Cu^{2+} and H50Q +Cu^{2+} are the less-damaging aggregates and the ones that promote to a larger extent inclusion formation. Although so far we cannot identify the causes of this fact, similar observations were previously reported (62–66). Inclusion bodies were demonstrated to be protective in the case of the Huntington's disease-related protein huntingtin (67). This was also observed in the case of nuclear huntingtin inclusions (68). Importantly, the nuclear aSyn inclusions we describe herein resemble those found in Huntington's disease-affected brains, given that they are ubiquitinated and have similar size and morphology (69).

It is also possible that aSyn species exert toxicity from the outside, without the need to enter the recipient cell. In that case, the most aggressive species would induce cell death, avoiding the lag time necessary to be internalized and trigger inclusion formation. Indeed, toxicity exerted by exogenous aSyn species has been reported, particularly in the case of aSyn oligomers (13). The disruption of membrane integrity and permeability is one of the possible molecular mechanisms involved (70); this could promote calcium influx and deregulation of cellular homeostasis (52). Although unlikely, because we used mature aggregates at the end point of the aggregation reaction, it is possible that the presence of residual oligomers in our samples may contribute to

the toxic effects observed. Finally, it is also possible that the intrinsic toxicity of the recombinant species hamper their own self-propagation. Recently, it was demonstrated that an increase in aSyn aggregation is not associated with stronger neuronal injury, arguing that efficient propagation of the protein is an active process, where healthy cellular metabolism and connections are necessary (61). In addition, injection of two different aSyn strains in vivo demonstrated that although both strains induce the formation of p-aSyn inclusions, this effect is reduced in the case of the most toxic strain, confirming that under certain conditions, there is an inverse correlation between seeding and damaging capacity (58).

In total, our study characterized the effects of various forms of aSyn aggregates in the intracellular milieu. Ultimately, the unambiguous dissociation between inclusion formation and toxicity will be essential to guide the development of future therapeutic approaches against synucleinopathies.

Materials and Methods

Purification of aSyn. aSyn WT and H50Q were produced as previously described (71, 72), using ammonium sulfate precipitation and ion-exchange chromatography. For further details, see *SI Appendix, SI Materials and Methods*.

Aggregation of aSyn. aSyn was aggregated at 70 μM in the presence or absence of $CuCl_2$ at 70 μM. Aggregation kinetics were conducted at 37 °C under agitation and followed by Th-T binding. Sedimentation assays were carried out by measuring the remaining soluble protein at the end time point of aggregation. Aggregation kinetics of aSyn in the presence of different Cu^{2+} concentrations and iron were performed in a 96-well plate with Teflon-balls, as previously described (73). For live cell imaging, aSyn aggregates were labeled with ATTO 590 NHS-ester (Atto-Tec) as previously described (50). For further details, see *SI Appendix, SI Materials and Methods*.

Circular Dichroism. CD spectra were obtained at a spectral resolution of 1 cm^{-1} and 15 $nm{\cdot}min^{-1}$ scan rate and collected over the 190- to 260-nm wavelength range at 25 °C using a Jasco 810 spectropolarimeter with a quartz cell of 0.1-cm path length. For the soluble state measurements, solutions at 10 μM were filtered through a 0.22-μM filter. At the end time point of aggregation, samples were diluted to 10 μM and vigorously homogenized in PBS before the measurements.

FTIR. ATR–FTIR spectra of the aSyn aggregates were obtained with Bruker Tensor 27 FTIR spectrometer (Bruker Optics). For further details, see *SI Appendix, SI Materials and Methods*.

ANS Binding Assays. The assays were performed by incubating 5 μM of aggregated samples with 20 μM of ANS in PBS. ANS fluorescence was measured on an ISS K2 spectrofluorometer. Samples were excited at 370 nm, and the emissions were collected from 400 to 600 nm using slits of 0.5 cm. The intensity at 374 nm was used to compare the extent of ANS bound to each sample. Assays with the soluble proteins were carried out by incubating 70 μM of the monomeric samples with 70 μM of ANS (soluble Transthyretin was used as positive control).

Transmission Electron Microscopy. Aggregated samples were adsorbed onto carbon-coated grids, rinsed with water, and stained with 2% (wt/vol) uranyl acetate. The samples were exhaustively scanned and representative fields were imaged in a Hitachi H-7000 TEM operating at an accelerating voltage of 75 kV.

PK Digestion Analysis. PK digestions of aSyn aggregates at the indicated time points were conducted at 37 °C. The resulting fragments were analyzed in Tricine-based protein electrophoresis. For further details, see *SI Appendix, SI Materials and Methods*.

NMR Spectroscopy. NMR experiments were recorded at 37 °C on a Bruker Avance 600 MHz spectrometer. To assess the seeding capabilities of different aggregates, a 4% concentration (vol/vol) of preformed aggregates, as described above WT $-Cu^{2+}$, WT $+Cu^{2+}$, H50Q $-Cu^{2+}$, H50Q $+Cu^{2+}$, were added to a 70-μM concentration of the fresh monomeric protein (in the absence or presence of an equimolar concentration of Cu^{2+}). The NMR buffer was 25 mM Hepes, 100 mM NaCl at pH 7.4, 90% H_2O/10% D_2O (vol/vol). ^1H NMR spectra were recorded every 2 h for at least 20 h after the addition of seeds. The reduction in signal intensity reports on the decrease in the concentration of monomeric protein.

Molecular Simulations. Details on the methodology are found in *SI Appendix, SI Molecular Simulations*.

Human Cell Cultures. Human H4 cells were treated, 24 h after transfection, with 1 μM of $CuCl_2$. For further details, see *SI Appendix, SI Materials and Methods*.

Primary Cell Cultures. Preparation of primary cortical cultures from WT rats was carried out as previously described (74). Cells were treated with 1 μM of aSyn aggregates. For live cell imaging, neurons were infected with a GFP-overexpressing lentivirus previous to the application of aSyn prelabeled aggregates. For further details, see *SI Appendix, SI Materials and Methods*.

Immunostaining Studies. Cells were fixed with paraformaldehyde and, when appropriate, with addition of 1% Triton X-100 to remove soluble structures (38). After permeabilization and blocking, cells were incubated with primary antibodies overnight at 4 °C and subsequently with Alexa Fluor-conjugated secondary antibodies. Leica DMI 6000B and Olympus XI81 microscopes were used for imaging. For further details, see *SI Appendix, SI Materials and Methods*.

Immunoblotting Analysis. Cells were lysed with a native buffer containing 1% Triton X-100 and cell debris was discarded by centrifugation. Cell lysates were separated in SDS/PAGE gels and transferred to blotting membranes, which were subsequently blocked with 5% (wt/vol) milk. Primary and secondary antibodies were incubated overnight at 4 °C and for 1 h at room temperature, respectively, and membranes were developed. For further details, see *SI Appendix, SI Materials and Methods*.

ACKNOWLEDGMENTS. We thank Prof. Dr. I. Ferrer for the nucleolin antibody; and Dr. N. Cook and Dr. N. Halbsgut for the assistance with confocal microscopy and image preparation, respectively. This research was supported by the European Community's Seventh Framework Programme FP7/2009 under Grant Agreement 238316. This study makes use of results or expertise provided by BioExcel CoE (www.bioexcel.eu), a project funded by the European Union Contract H2020-EINFRA-2015-1-675728. A.V.-P. was funded by the Dorothea Schlözer Programme of the Georg August University Göttingen; T.L. d.F. was funded by Fundação para a Ciência e Tecnologia (SFRH/BD/74881/2010); R.S. was funded by Comissao de Aperfeiçoamento de Pessoal de Nival Superior–Science without Borders and CNPq; R.P. was funded by Fundação para a Ciência e Tecnologia (SFRH/BD/80884/2011); É.M.S. was funded by the Dorothea Schlözer Programme of the Georg August University Göttingen; E.A.G. was funded by the Deutsche Forschungsgemeinschaft (DFG) grant "Copper binding to the physiological form of the α-synuclein protein"; I.M. was funded by an Emmy Noether/DFG grant; S.V. is supported by the Catalan Institution for Research and Advanced Studies-Academia program; and T.F.O. is supported by the DFG Center for Nanoscale Microscopy and Molecular Physiology of the Brain.

1. McCann H, Stevens CH, Cartwright H, Halliday GM (2014) α-Synucleinopathy phenotypes. *Parkinsonism Relat Disord* 20(Suppl 1):S62–S67.
2. Pasanen P, et al. (2014) Novel α-synuclein mutation A53E associated with atypical multiple system atrophy and Parkinson's disease-type pathology. *Neurobiol Aging* 35(9):2180.e1–2180.e5.
3. Xu W, Tan L, Yu J-T (2015) Link between the SNCA gene and parkinsonism. *Neurobiol Aging* 36(3):1505–1518.
4. Maroteaux L, Campanelli JT, Scheller RH (1988) Synuclein: A neuron-specific protein localized to the nucleus and presynaptic nerve terminal. *J Neurosci* 8(8):2804–2815.
5. Breydo L, Wu JW, Uversky VN (2012) Alpha-synuclein misfolding and Parkinson's disease. *Biochim Biophys Acta* 1822(2):261–285.
6. Burré J, Sharma M, Südhof TC (2014) α-Synuclein assembles into higher-order multimers upon membrane binding to promote SNARE complex formation. *Proc Natl Acad Sci USA* 111(40):E4274–E4283.
7. Spillantini MG, Crowther RA, Jakes R, Hasegawa M, Goedert M (1998) Alpha-synuclein in filamentous inclusions of Lewy bodies from Parkinson's disease and dementia with Lewy bodies. *Proc Natl Acad Sci USA* 95(11):6469–6473.
8. Fujiwara H, et al. (2002) Alpha-synuclein is phosphorylated in synucleinopathy lesions. *Nat Cell Biol* 4(2):160–164.
9. Gómez-Tortosa E, Irizarry MC, Gómez-Isla T, Hyman BT (2000) Clinical and neuropathological correlates of dementia with Lewy bodies. *Ann N Y Acad Sci* 920: 9–15.
10. Dickson DW (2012) Parkinson's disease and parkinsonism: Neuropathology. *Cold Spring Harb Perspect Med* 2(8):a009258.
11. Cookson MR, van der Brug M (2008) Cell systems and the toxic mechanism(s) of alpha-synuclein. *Exp Neurol* 209(1):5–11.
12. Eisbach SE, Outeiro TF (2013) Alpha-synuclein and intracellular trafficking: impact on the spreading of Parkinson's disease pathology. *J Mol Med (Berl)* 91(6):693–703.

13. Roberts HL, Brown DR (2015) Seeking a mechanism for the toxicity of oligomeric α-synuclein. *Biomolecules* 5(2):282–305.
14. Winner B, et al. (2011) In vivo demonstration that alpha-synuclein oligomers are toxic. *Proc Natl Acad Sci USA* 108(10):4194–4199.
15. Karpinar DP, et al. (2009) Pre-fibrillar alpha-synuclein variants with impaired beta-structure increase neurotoxicity in Parkinson's disease models. *EMBO J* 28(20):3256–3268.
16. Braak H, et al. (2003) Staging of brain pathology related to sporadic Parkinson's disease. *Neurobiol Aging* 24(2):197–211.
17. Li J-Y, et al. (2008) Lewy bodies in grafted neurons in subjects with Parkinson's disease suggest host-to-graft disease propagation. *Nat Med* 14(5):501–503.
18. Angot E, Brundin P (2009) Dissecting the potential molecular mechanisms underlying alpha-synuclein cell-to-cell transfer in Parkinson's disease. *Parkinsonism Relat Disord* 15(Suppl 3):S143–S147.
19. Masuda-Suzukake M, et al. (2013) Prion-like spreading of pathological α-synuclein in brain. *Brain* 136(Pt 4):1128–1138.
20. Recasens A, et al. (2014) Lewy body extracts from Parkinson disease brains trigger α-synuclein pathology and neurodegeneration in mice and monkeys. *Ann Neurol* 75(3):351–362.
21. Gorell JM, et al. (1999) Occupational exposure to manganese, copper, lead, iron, mercury and zinc and the risk of Parkinson's disease. *Neurotoxicology* 20(2-3):239–247.
22. Willis AW, et al. (2010) Metal emissions and urban incident Parkinson disease: A community health study of Medicare beneficiaries by using geographic information systems. *Am J Epidemiol* 172(12):1357–1363.
23. Santner A, Uversky VN (2010) Metalloproteomics and metal toxicology of α-synuclein. *Metallomics* 2(6):378–392.
24. Kozlowski H, et al. (2009) Copper, iron, and zinc ions homeostasis and their role in neurodegenerative disorders (metal uptake, transport, distribution and regulation). *Coord Chem Rev* 253(21-22):2665–2685.
25. Uversky VN, Li J, Fink AL (2001) Metal-triggered structural transformations, aggregation, and fibrillation of human alpha-synuclein. A possible molecular NK between Parkinson's disease and heavy metal exposure. *J Biol Chem* 276(47):44284–44296.
26. Rasia RM, et al. (2005) Structural characterization of copper(II) binding to alpha-synuclein: Insights into the bioinorganic chemistry of Parkinson's disease. *Proc Natl Acad Sci USA* 102(12):4294–4299.
27. Jarrett JT, Lansbury PT, Jr (1993) Seeding "one-dimensional crystallization" of amyloid: A pathogenic mechanism in Alzheimer's disease and scrapie? *Cell* 73(6):1055–1058.
28. Rose F, Hodak M, Bernholc J (2011) Mechanism of copper(II)-induced misfolding of Parkinson's disease protein. *Sci Rep* 1:11.
29. Sóvágó I, Kállay C, Várnagy K (2012) Peptides as complexing agents: Factors influencing the structure and thermodynamic stability of peptide complexes. *Coord Chem Rev* 256(19–20):2225–2233.
30. Kowalik-Jankowska T, Rajewska A, Jankowska E, Grzonka Z (2006) Copper(II) binding by fragments of alpha-synuclein containing M1-D2- and -H50-residues; a combined potentiometric and spectroscopic study. *Dalton Trans* (42):5068–5076.
31. Rossetti G, et al. (2016) Conformational ensemble of human α-synuclein physiological form predicted by molecular simulations. *Phys Chem Chem Phys* 18(8):5702–5706.
32. Berendsen HJC, Postma JPM, van Gunsteren WF, DiNola A, Haak JR (1984) Molecular dynamics with coupling to an external bath. *J Chem Phys* 81(8):3684–3690.
33. Valensin D, Dell'Acqua S, Kozlowski H, Casella L (April 11, 2016) Coordination and redox properties of copper interaction with α-synuclein. *J Inorg Biochem*, 10.1016/j.jinorgbio.2016.04.012.
34. Nosé S (1984) A molecular dynamics method for simulations in the canonical ensemble. *Mol Phys* 52(2):255–268.
35. Kosik KS, Finch EA (1987) MAP2 and tau segregate into dendritic and axonal domains after the elaboration of morphologically distinct neurites: An immunocytochemical study of cultured rat cerebrum. *J Neurosci* 7(10):3142–3153.
36. Sacino AN, et al. (2014) Brain injection of α-synuclein induces multiple proteinopathies, gliosis, and a neuronal injury marker. *J Neurosci* 34(37):12368–12378.
37. Pekny M, Pekna M (2014) Astrocyte reactivity and reactive astrogliosis: Costs and benefits. *Physiol Rev* 94(4):1077–1098.
38. Volpicelli-Daley LA, et al. (2011) Exogenous α-synuclein fibrils induce Lewy body pathology leading to synaptic dysfunction and neuron death. *Neuron* 72(1):57–71.
39. Sacino AN, et al. (2013) Conformational templating of α-synuclein aggregates in neuronal-glial cultures. *Mol Neurodegener* 8:17.
40. Uryu K, et al. (2006) Convergence of heat shock protein 90 with ubiquitin in filamentous alpha-synuclein inclusions of alpha-synucleinopathies. *Am J Pathol* 168(3):947–961.
41. Hasegawa M, et al. (2002) Phosphorylated alpha-synuclein is ubiquitinated in alpha-synucleinopathy lesions. *J Biol Chem* 277(50):49071–49076.
42. De Ricco R, et al. (2015) Remote His50 acts as a coordination switch in the high-affinity N-terminal centered copper(II) site of α-synuclein. *Inorg Chem* 54(10):4744–4751.
43. Wang X, Moualla D, Wright JA, Brown DR (2010) Copper binding regulates intracellular alpha-synuclein localisation, aggregation and toxicity. *J Neurochem* 113(3):704–714.
44. Xiang W, et al. (2015) Posttranslational modification and mutation of histidine 50 trigger alpha synuclein aggregation and toxicity. *Mol Neurodegener* 10(1):8.
45. Carboni E, Lingor P (2015) Insights on the interaction of alpha-synuclein and metals in the pathophysiology of Parkinson's disease. *Metallomics* 7(3):395–404.
46. Qin Z, Hu D, Han S, Hong D-P, Fink AL (2007) Role of different regions of alpha-synuclein in the assembly of fibrils. *Biochemistry* 46(46):13322–13330.
47. Binolfi A, et al. (2011) Exploring the structural details of Cu(I) binding to α-synuclein by NMR spectroscopy. *J Am Chem Soc* 133(2):194–196.
48. Danzer KM, Krebs SK, Wolff M, Birk G, Hengerer B (2009) Seeding induced by alpha-synuclein oligomers provides evidence for spreading of alpha-synuclein pathology. *J Neurochem* 111(1):192–203.
49. Luk KC, et al. (2009) Exogenous alpha-synuclein fibrils seed the formation of Lewy body-like intracellular inclusions in cultured cells. *Proc Natl Acad Sci USA* 106(47):20051–20056.
50. Hansen C, et al. (2011) α-Synuclein propagates from mouse brain to grafted dopaminergic neurons and seeds aggregation in cultured human cells. *J Clin Invest* 121(2):715–725.
51. Volpicelli-Daley LA, Luk KC, Lee VM-Y (2014) Addition of exogenous α-synuclein preformed fibrils to primary neuronal cultures to seed recruitment of endogenous α-synuclein to Lewy body and Lewy neurite-like aggregates. *Nat Protoc* 9(9):2135–2146.
52. Danzer KM, et al. (2007) Different species of alpha-synuclein oligomers induce calcium influx and seeding. *J Neurosci* 27(34):9220–9232.
53. Bousset L, et al. (2013) Structural and functional characterization of two alpha-synuclein strains. *Nat Commun* 4:2575.
54. Aulić S, et al. (2014) Defined α-synuclein prion-like molecular assemblies spreading in cell culture. *BMC Neurosci* 15:69.
55. Lee HJ, et al. (2010) Direct transfer of alpha-synuclein from neuron to astroglia causes inflammatory responses in synucleinopathies. *J Biol Chem* 285(12):9262–9272.
56. Schell H, Hasegawa T, Neumann M, Kahle PJ (2009) Nuclear and neuritic distribution of serine-129 phosphorylated α-synuclein in transgenic mice. *Neuroscience* 160(4):796–804.
57. Osterberg VR, et al. (2015) Progressive aggregation of alpha-synuclein and selective degeneration of Lewy inclusion-bearing neurons in a mouse model of parkinsonism. *Cell Reports* 10(8):1252–1260.
58. Peelaerts W, et al. (2015) α-Synuclein strains cause distinct synucleinopathies after local and systemic administration. *Nature* 522(7556):340–344.
59. Zhang S, et al. (2015) LK6/Mnk2a is a new kinase of alpha synuclein phosphorylation mediating neurodegeneration. *Sci Rep* 5:12564.
60. Outeiro TF, et al. (2008) Formation of toxic oligomeric alpha-synuclein species in living cells. *PLoS One* 3(4):e1867.
61. Ulusoy A, et al. (2015) Neuron-to-neuron α-synuclein propagation in vivo is independent of neuronal injury. *Acta Neuropathol Commun* 3(1):13.
62. Tanaka M, et al. (2004) Aggresomes formed by alpha-synuclein and synphilin-1 are cytoprotective. *J Biol Chem* 279(6):4625–4631.
63. Paine MG, Babu JR, Seibenhener ML, Wooten MW (2005) Evidence for p62 aggregate formation: Role in cell survival. *FEBS Lett* 579(22):5029–5034.
64. Bodner RA, et al. (2006) Pharmacological promotion of inclusion formation: A therapeutic approach for Huntington's and Parkinson's diseases. *Proc Natl Acad Sci USA* 103(11):4246–4251.
65. Smith WW, et al. (2010) Synphilin-1 attenuates neuronal degeneration in the A53T alpha-synuclein transgenic mouse model. *Hum Mol Genet* 19(11):2087–2098.
66. Fox LM, et al. (2011) Soluble tau species, not neurofibrillary aggregates, disrupt neural system integration in a tau transgenic model. *J Neuropathol Exp Neurol* 70(7):588–595.
67. Arrasate M, Mitra S, Schweitzer ES, Segal MR, Finkbeiner S (2004) Inclusion body formation reduces levels of mutant huntingtin and the risk of neuronal death. *Nature* 431(7010):805–810.
68. Saudou F, Finkbeiner S, Devys D, Greenberg ME (1998) Huntingtin acts in the nucleus to induce apoptosis but death does not correlate with the formation of intranuclear inclusions. *Cell* 95(1):55–66.
69. Sieradzan KA, et al. (1999) Huntington's disease intranuclear inclusions contain truncated, ubiquitinated huntingtin protein. *Exp Neurol* 156(1):92–99.
70. Butterfield SM, Lashuel HA (2010) Amyloidogenic protein-membrane interactions: Mechanistic insight from model systems. *Angew Chem Int Ed Engl* 49(33):5628–5654.
71. Volles MJ, Lansbury PT, Jr (2007) Relationships between the sequence of alpha-synuclein and its membrane affinity, fibrillization propensity, and yeast toxicity. *J Mol Biol* 366(5):1510–1522.
72. Chutna O, et al. (2014) The small GTPase Rab11 co-localizes with α-synuclein in intracellular inclusions and modulates its aggregation, secretion and toxicity. *Hum Mol Genet* 23(25):6732–6745.
73. Giehm L, Lorenzen N, Otzen DE (2011) Assays for α-synuclein aggregation. *Methods* 53(3):295–305.
74. Tönges L, et al. (2014) Alpha-synuclein mutations impair axonal regeneration in models of Parkinson's disease. *Front Aging Neurosci* 6:239.
75. Susi H, Byler DM (1983) Protein structure by Fourier transform infrared spectroscopy: Second derivative spectra. *Biochem Biophys Res Commun* 115(1):391–397.